The Effects of Lewis Number on the Combustion Limit, Near-Limit Extinction Boudary, and Flame Regimes of Low-Lewis-Number Counterflow Flames under Microgravity

Tomoya Okuno[1], Hisashi Nakamura[1], Takuya Tezuka[1], Susumu Hasegawa[1], Masao Kikuchi[2], Kaoru Maruta[1,3]

[1]Institute of Fluid Science, Tohoku University, Sendai, Miyagi, Japan

[2]Japan Aerospace Exploration Agency, Tsukuba, Ibaraki, Japan

[3]Far Eastern Federal University, Russky Island, Russia

1 Introduction

A complete and comprehensive understanding on the combustion limits of near-limit stretched premixed flames has not been achieved for low-Lewis-number flames, despite extensive efforts of many researchers. The combustion limits of premixed flames have been widely studied using the counterflow flame configuration for within the range of Lewis numbers (*Le*) from 0.97 to 1.8 in [1-6]. Meanwhile, theoretical, computational, and experimental investigations revealed that spherical flames which do not propagate, flame balls, may exist below the lean flammability limit of a normal planar propagating flame due to the *Le* effect [7]. However, since the propagating flame and the flame ball were investigated separately, the relationship between these two flame types was not fully elucidated. A recent study by our group has shown that transitions to ball-like flames from counterflow planar flames occur for $CH_4/O_2/Xe$ mixtures both experimentally and computationally [8, 9]. In the previous study [9], computational flame regimes and the extension of the combustion limit due to the formation of multiple ball-like flames, termed sporadic flames, were obtained. Counterflow experiments with $CH_4/O_2/CO_2$ mixtures have also shown the experimental flame regimes for $Le = 0.75$ with a significant effect of radiation reabsorption [10]. However, the effects of *Le* on the combustion limit, formation of the ball-like flames, and the flame regimes have not been investigated yet. Therefore, in this study, we have conducted investigations on this effect by using Kr or Xe gas as a diluent for methane flames to change the *Le*.

2 Experimental and computational method

Correspondence to: okuno@edyn.ifs.tohoku.ac.jp

A schematic of the employed experimental apparatus is shown in Fig. 1. Microgravity environment was obtained by a parabolic flight of an airplane (MU-300) which was operated by the Diamond Air Service Company, Japan. The gravity levels were on the order of ±0.01 G. Two opposing burners were placed inside a chamber. Here, the burner diameter was 3.0 cm and the burner distance was varied between 3.0‑4.5 cm to avoid conductive heat loss from the flames to the burners. The detailed structure of the burners can be obtained from [1]. $CH_4/O_2/Kr$ or $CH_4/O_2/Xe$ premixtures were supplied to both burners, forming a counterflow field. The mole fraction ratio of O_2 to the diluent in the mixture was 0.141. *Le* for Xe and Kr diluted mixtures were around 0.5 and 0.75, respectively. After ignition, the equivalence ratio and/or the stretch rate were gradually changed to obtain the extinction point. Here, the stretch rate, a, was defined as $2U/L$ where U is the mean velocity at the burner outlet and L is the burner distance. For most cases, the stretch rate was kept constant and the equivalence ratio was gradually decreased by 0.01 per second. Experiments were conducted in the range of stretch rates from 0.8 to 6.5 s^{-1}. For flame observation, two HD cameras and a high-speed camera equipped with an image intensifier were used. Extinction was defined as the instantaneous equivalence ratio when the chemiluminescence vanished in the camera image.

Ideal one-dimensional counterflow computations were conducted to obtain the extinction curve and compare with the experiments. A computational code for the counterflow geometry modified from PREMIX was used [3]. The optically thin model was used for the radiation heat loss [3]. All computations were conducted under atmospheric pressure and the chemistry was taken from GRI-Mech 3.0 [11] with reactions related to N removed.

Three-dimensional transient computations using the diffusive-thermal model used in [9] were employed to obtain the flame configurations. Non-dimensional equations describing the concentration and the temperature were solved with the constant density assumption. The computed domain was set to be $-40 \leqq X \leqq 40$, $-30 \leqq Y \leqq 30$, and $-40 \leqq Z \leqq 40$, where the coordinates were non-dimensionalized by D_{th}/U_b. Here, D_{th} is the thermal diffusion coefficient and U_b is the laminar burning velocity. In the 3-D computations, the mixtures were supplied from the plane $Y = -30$ and $Y = 30$, and the velocity field V was prescribed such that $V = (AX/2, -AY, AZ/2)$. Here A is the non-dimensional stretch rate where time was non-dimensionalized by U_b^2/D_{th}. For the chemistry, we have employed the single reactant one-step Arrhenius-type exothermic reaction for fuel-lean mixtures. The activation temperature and the pre-exponential factor in the reaction rate term were fitted to the adiabatic flame temperature, T_b, using the relations $T_b(\phi)$ and $U_b(\phi)$ which were computed by GRI-Mech 3.0 in the range of equivalence ratios from 0.38 to 0.6 for $CH_4/O_2/Xe$ mixtures.

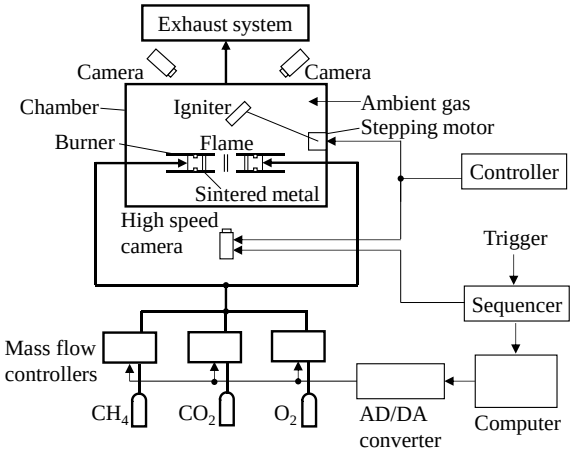

Fig. 1 Schematic of the experimental apparatus.

Using these relations, the non-dimensional fuel concentration and stretch rate are converted to dimensional parameters.

3 Experimental and computational results

The experimental flame configurations obtained for $\phi = 0.48$ with $CH_4/O_2/Xe$ mixtures at $a = 0.8$, 2.2, and 3.2 s^{-1} and with $CH_4/O_2/Kr$ mixtures at $a = 2.1$ and 3.2 s^{-1} are shown in Fig. 2. At $a = 3.2$ s^{-1} for Xe and Kr mixtures, planar flames are obtained. At $a = 2.1$ s^{-1} for Kr mixtures, planar flames are observed, while for Xe mixtures at $a = 2.2$ s^{-1}, wrinkled flames with a continuous flame front called cellular flames are observed. The differences in the flame configurations are due to the diffusive-thermal instability, where the $Le = 0.5$ for Xe mixtures and $Le = 0.75$ for Kr mixtures. At $a = 0.82$ s^{-1} for Xe mixtures, each of the cells are separated which leads to reactant leakage to the stagnation plane. These flames are called sporadic flames and has been predicted by computations with the diffusive-thermal model in [9]. For Kr mixtures, cellular flames and sporadic flames were not observed regardless of the stretch rate at $\phi = 0.48$.

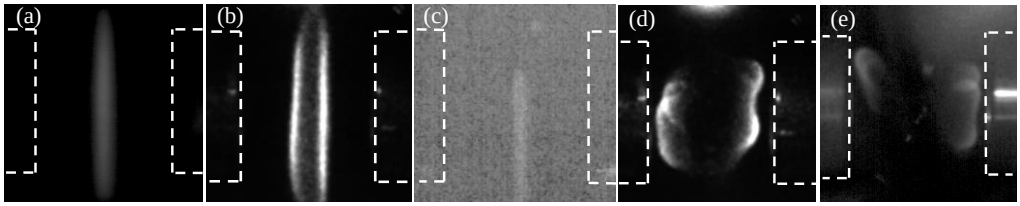

Fig. 2 Experimental flame configurations at $\phi = 0.48$. (a) $CH_4/O_2/Kr$, $a = 3.2$ s^{-1}, (b) $CH_4/O_2/Xe$, $a = 3.2$ s^{-1}, (c) $CH_4/O_2/Kr$, $a = 2.1$ s^{-1}, (d) $CH_4/O_2/Xe$, $a = 2.2$ s^{-1}, (e) $CH_4/O_2/Xe$, $a = 0.82$ s^{-1}.

In addition to the flame configurations shown in Fig. 2, three types of extinction behaviors for planar flames were observed. One type is the normal planar flame extinction where the instantaneous disappearance of the luminous zone from all regions occur. The second type is shown in Fig. 3a where the merged edges of the planar circular flames move downstream, propagating toward the mixture of burnt and unburnt gas. The third type is shown in Fig. 3b where the merged edges of the planar circular flame move upstream, retreating toward the burnt gas. Just before extinction, the appearance of the flame is similar to a flattened ball-like flame.

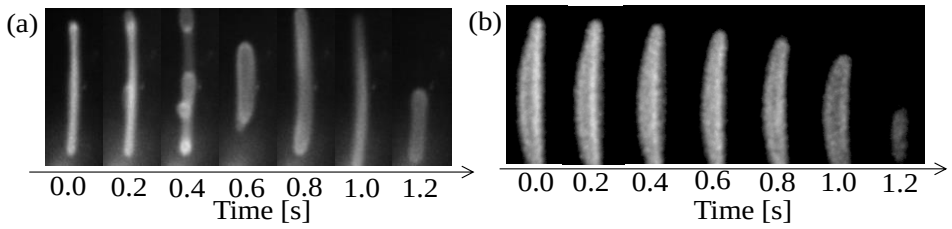

Fig. 3 Behavior of near-limit planar flames of $CH_4/O_2/Xe$ mixtures. (a) Planar circular flames with propagating edges at $a = 2.6$ s^{-1} and around $\phi = 0.50$. (b) Planar circular flames with retreating edges at $a = 2.2$ s^{-1} and around $\phi = 0.38$.

Computational isosurfaces at $T = 0.85$ and fuel concentration contours along the burner axis are shown in Fig. 4. Here, T is the temperature which was non-dimensionalized by the adiabatic flame temperature and the fuel concentration, C, was non-dimensionalized by the inlet fuel concentration. In dimensional coordinates, the computed domain size is from $-9.2 \leqq x$ (cm) $\leqq 9.2$, $-6.9 \leqq y$ (cm) $\leqq 6.9$, and $-9.2 \leqq z$ (cm) $\leqq 9.2$ at $\phi = 0.48$. Note that this dimension size changes with equivalence ratio. At $\phi = 0.48$ and $a =$

1.0 s^{-1}, the flames are planar for both *Le* = 0.5 and 0.75 conditions as shown in Fig. 4a and Fig. 4b, respectively. This is in qualitative agreement to the results shown in Fig. 4a and Fig. 4b. However, when the stretch rate is decreased from 1.0 s^{-1} to 0.18 s^{-1}, reactant leakage is observed and sporadic flames are formed for the case of *Le* = 0.5 as shown in Fig. 4c. In this case, each cell is formed, split, and swept away, resulting in a quasi-steady flame front. For the case of *Le* = 0.75, the flames remained planar and extinguished from all zones around 0.8 s^{-1} when the stretch rate was decreased, although the results are not shown here. The formation of sporadic flames for *Le* = 0.5 and the formation of only planar flames for *Le* = 0.75 are in qualitative agreements with the experimental results. However, planar circular flames with

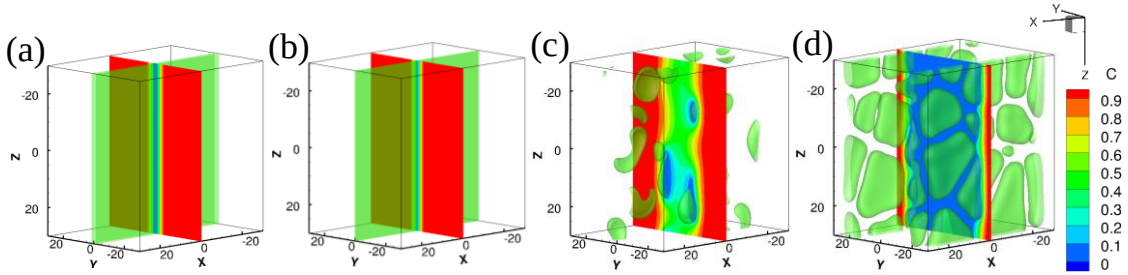

Fig. 4 Computational isosurfaces at T = 0.85 and fuel concentration contours along the burner axis. (a) *Le* = 0.75, ϕ = 0.48, a = 1.0 s^{-1}, (b) *Le* = 0.5, ϕ = 0.48, a = 1.0 s^{-1}, (c) *Le* = 0.5, ϕ = 0.48, a = 0.18 s^{-1}, (d) *Le* = 0.5, ϕ = 0.50, a = 0.18 s^{-1}.

merged edges could not be observed in the current computations. When the equivalence ratio was increased from ϕ = 0.48 to 0.50, the sporadic flames turned into cellular flames with no reactant leakage along the stagnation plane at a = 0.18 s^{-1} and *Le* = 0.5 as shown in Fig 3(d). This flame configuration is in qualitative agreement with the result shown in Fig 2d.

To experimentally observe the behavior of the sporadic flames, the fuel and concentration was kept almost constant at a = 0.8 s^{-1} and ϕ = 0.39, as shown in Fig. 5. Instantaneous flame images obtained in experiments are also shown in Fig. 5. It can be seen here that a sporadic structure was formed for over 6.0 s, which indicates that the sporadic flame structure may be stable.

The extinction points (×) obtained by microgravity experiments and 1-D computations are shown in Figs. 6a and 6b, and the experimental flame regimes are shown in Figs. 6c and 6d. For Kr diluted mixtures, the experimental results agree with the 1-D computational result, as shown in Fig. 6a. At lower stretch rates, a region exists where extinction at higher equivalence ratios than the C-shaped curve occurs. This is due to the flame bifurcation, where flames which stand far apart and close together could be observed at the same equivalence ratio and stretch rate conditions. This is in qualitative agreement to the G-shaped extinction

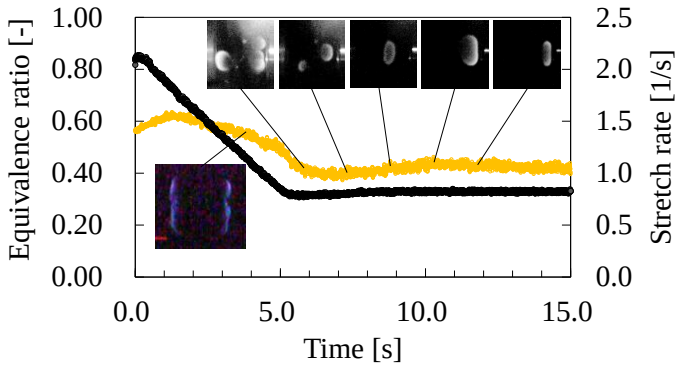

Fig. 5 Experimental behavior of sporadic flames at a = 0.8 s^{-1} and ϕ = 0.4 for $CH_4/O_2/Xe$ mixtures.

curve which was obtained computationally by Ju et al [3]. For Xe mixtures, the extinction points are more scattered compared to Kr mixtures. This is likely due to the stronger *Le* effect. Qualitative agreement between the experimental extinction points and the 1-D computational extinction curve from stretch rates 1.6 to 6.0 s^{-1} is seen for Xe mixtures. However, at stretch rates around 0.8 s^{-1}, particularly large differences between the experimental extinction points and the 1-D computational extinction curve are seen. Comparing Figs. 6c and 6d, it can be seen that the regime for sporadic flames exist only for Xe mixtures. This indicates that sporadic flames can be formed for mixtures at *Le* = 0.5 where sporadic flames cannot be formed for mixtures at *Le* = 0.75. This is in qualitative agreement with the 3-D computational results, where sporadic flames could be observed at *Le* = 0.5 while they could not be observed at *Le* = 0.75. The region of sporadic flames also coincide with the region where particularly large differences between the experimental extinction points and the 1-D computations are observed. This behavior is in qualitative agreement with the previous results obtained in [9]. Comparing Fig. 6c and Fig. 6d, it can also be seen that the region of cellular flames is extended to lower equivalence ratios for Xe mixtures compared to Kr mixtures. This is because Xe mixtures have a smaller *Le* which results in a stronger diffusive-thermal instability which produces cellular flames. Also for relatively higher stretch rates, the planar circular flames with propagating edges are seen, whereas for relatively lower stretch rates, the planar circular flames with receding edges are seen. This means that the merged edges of the planar circular flames have both positive and negative propagation speeds depending on the stretch rate.

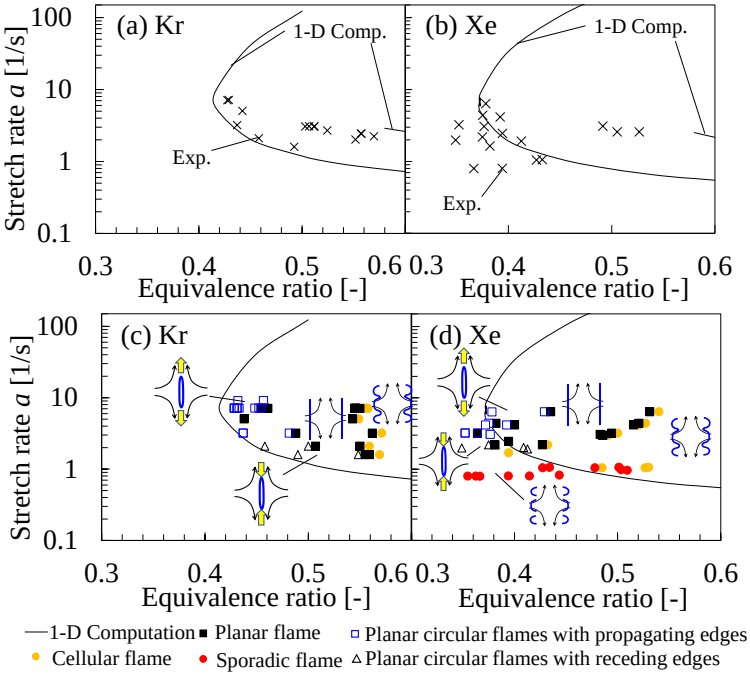

Fig. 6 Experimental extinction points for (a) $CH_4/O_2/Kr$ mixtures and (b) $CH_4/O_2/Xe$ mixtures. Experimental flame regimes for (c) $CH_4/O_2/Kr$ mixtures and (d) $CH_4/O_2/Xe$ mixtures.

4 Conclusions

Microgravity counterflow experiments and 1-D counterflow computations with detailed chemistry for $CH_4/O_2/Kr$ (*Le* = 0.75) and $CH_4/O_2/Xe$ (*Le* = 0.50) mixtures, and 3-D transient computations using the diffusive-

thermal model showed the following conclusions. Planar flames were seen for both *Le* = 0.5 and 0.75 mixtures at relatively higher stretch rates and ϕ = 0.48, experimentally. With decreasing stretch rates, cellular and sporadic flames were observed for mixtures at *Le* = 0.5 while only planar flames were observed for mixtures at *Le* = 0.75 experimentally in the case of ϕ = 0.48. At *Le*= 0.75 and ϕ = 0.48, only planar flames are observed in the 3-D computations. At *Le* = 0.5, planar flames at higher stretch rates and sporadic flames at lower stretch rates were observed in the 3-D computations. Flame bifurcations were seen at low stretch rates which resulted in a G-shaped extinction curve experimentally and computationally. In addition, particularly large differences between the 1-D computational extinction curve and the experimental extinction limits were seen around $a = 0.8\ s^{-1}$. This region coincides with the region of sporadic flames, which is in qualitative agreement with the 3-D computational results in [9].

Acknowledgement

The authors would like to thank Prof. Sergey Minaev and Dr. Roman Fursenko of Far Eastern Federal University, for helpful suggestions concerning the diffusive-thermal model and the 3-D computations.

References

[1] Maruta K, Yoshida M, Ju Y, Niioka T. (1996). Experimental study on methane-air premixed flame extinction at small stretch rates in microgravity. Symp. (Int.) Combust. 26: 1283.
[2] Maruta K, Ju Y, Honda A, Niioka T. (1998). Lewis number effect on extinction characteristics of radiative counterflow CH4/O2/N2/He flames. Symp. (Int.) Combust. 27: 2611.
[3] Ju Y, Guo H, Maruta K, Liu F. (1997). On the extinction limit and flammability limit of counterflow non-adiabatic stretched methane-air premixed flames. J. Fluid Mech. 342: 315.
[4] Ju Y, Guo H, Maruta K, Niioka T. (1998). Flame bifurcation and flammable regions of radiative counterflow premixed flames with general Lewis numbers. Combust. Flame 113: 603.
[5] Sung CJ, Law CK. (1996). Extinction mechanisms of near-limit premixed flames and extended limits of flammability. Symp. (Int.) Combust. 26: 865.
[6] Buckmaster JD. (1997). The effects of radiation on stretched flames. Combust. Theory Model. 1: 1.
[7] Ronney PD, Wu M-S, Pearlman HG, Weiland KJ. (1998). Structure of flame balls at low Lewis-number (SOFBALL): Preliminary results from the STS-83 space flight experiments. AIAA J. 36: 1361.
[8] Takase K, Li X, Nakamura H, Kikuchi M, Maruta K. (2013). Extinction characteristics of CH4/O2/Xe radiative counterflow planar premixed flames and their transition to ball-like flames, Combust. Flame 160: 1235.
[9] Fursenko R, Minaev S, Nakamura H, Tezuka T, Hasegawa S, Kobayashi T, Takase K, Katsuta M, Kikuchi M, Maruta K. (2015). Near-lean limit combustion regimes of low-Lewis-number stretched premixed flames, Combust. Flame 162: 1712.
[10]Okuno T, Nakamura H, Tezuka T, Hasegawa S, Takase T, Katsuta M, Kikuchi M, Maruta K. (2016). Study on the combustion limit, near-limit extinction boundary, and flame regimes of low-Lewis-number CH4/O2/CO2 counteflow flames under microgravity. Combust. Flame 172: 13.
[11] Smith GP, Golden DM, Frenklach M, Moriarty NW, Eiteneer B, Goldenberg M, Bowman CT, Hanson RK, Song S, Gardiner Jr. WC, Lissianki V, Quin Z. (2002). <http://ww w.me.berkeley.edu/gri_mech>.